J. Cent. South Univ. (2021) 28: 1−15
DOI: https://doi.org/10.1007/s11771-020-4504-x

Springer

Microstructure and Gd-rich phase evolution of as-cast AZ31-*x*Gd magnesium alloys during semi-solid isothermal heat treatment

CHU Chen-liang(褚晨亮)[1], WU Xiao-quan(吴孝泉)[1], QIU Shui-cai(邱水才)[2], TANG Bin-bing(汤斌兵)[3], YIN Zheng(殷正)[1], YAN Hong(闫洪)[1], LUO Chao(罗超)[3], HU Zhi(胡志)[1]

1. Institute of Advanced Forming, Nanchang University, Nanchang 330031, China;
2. Changzhou University Huaide College, Jingjiang 214513, China;
3. Institute for Advanced Study, Nanchang University, Nanchang 330031, China

Abstract: The microstructure and Gd-rich phase evolution of as-cast AZ31-*x*Gd (*x*=0, 1.5 wt.%, 2.0 wt.% and 2.5 wt.%) magnesium alloys during semi-solid isothermal heat treatment were investigated deeply in the present work. Results showed that the lamellar $(Mg,Al)_3Gd$ phases transformed into the particle-like Al_2Gd phases in AZ31 magnesium alloys with Gd addition during semi-solid isothermal heat treatment, leading to yielding more spherical *α*-Mg grains. When Gd content is 2.0 wt. %, the size of semi-solid spherical grains reaches the minimum. The main mechanism of grain refinement lies in the remelting of dendritic branches as well as the auxiliary effect of a small number of Al_2Gd particles as grain refining inoculants. Meanwhile, Al_2Gd particles enriched at the solid-liquid interfaces can remarkably retard the growth rate of *α*-Mg grains. A reduction of deformation resistance has been successfully achieved in AZ31-2.0Gd magnesium alloy after semi-solid isothermal heat treatment, which shows a moderate compressive deformation resistance (230 MPa), comparing to the as-cast AZ31 magnesium alloy (280 MPa) and semi-solid AZ31 magnesium alloy (209 MPa).

Key words: magnesium; microstructure; rare earth element; Al_2Gd particle; semi-solid isothermal heat treatment

Cite this article as: CHU Chen-liang, WU Xiao-quan, QIU Shui-cai, TANG Bin-bing, YIN Zheng, YAN Hong, LUO Chao, HU Zhi. Microstructure and Gd-rich phase evolution of as-cast AZ31-*x*Gd magnesium alloys during semi-solid isothermal heat treatment [J]. Journal of Central South University, 2021, 28(1): 1−15. DOI: https://doi.org/10.1007/s11771-020-4504-x.

1 Introduction

In addition to having the lowest density (approximately 1/4 iron and 2/3 aluminum) of structural materials, Mg alloys possess advantages of a high strength-to-weight ratio, good electrical conductivity, and easy machining, leading to increasing applications in aerospace, automobiles, and 3C products [1, 2]. However, poor high-temperature strength and plastic-forming abilities have restricted applications of these alloys. Recent studies have found that RE elements could improve the mechanical properties and thermal stability of magnesium alloys due to the precipitation strengthening, fine-grain strengthening and LPSO strengthening [3−5]. Accordingly, various LPSO-containing Mg-RE alloys with superior mechanical properties have been developed, such as low-cost $Mg_{88}Zn_4Y_7$ alloy and $Mg_{96.82}Gd_2Zn_1Zr_{0.18}$ alloy [6].

Foundation item: Project(20171BAB206005) supported by the Natural Science Foundation of Jiangxi Province, China; Project(20153BCB23023) supported by the Training Program Foundation for Young Scientists of Jiangxi Province, China; Project(51961026) supported by the National Natural Science Foundation of China
Received date: 2020-03-18; **Accepted date:** 2020-06-08
Corresponding author: HU Zhi, PhD, Associate Professor; Tel: +86-791-83969633; E-mail: huzhi@ncu.edu.cn; ORCID: https://orcid.org/0000-0003-4148-5107

Among various manufacturing approaches, the semi-solid forming process has provided a new means of addressing drawbacks related to the plastic-forming abilities of wrought Mg alloys, such as AZ31 and AZ61, of which thixoforming is widely accepted due to the simple formation process [7−10]. To obtain a fine and globular semi-solid non-dendritic structure is the foundation of thixoforming technology. Many methods have been used to obtain semi-solid non-dendritic materials, including mechanical and electromagnetic stirring and ultrasonic vibration [11]. Recent reports have indicated that isothermal heat treatment can facilitate the evolution of dendrites into spherical grains during secondary heating prior to pressure formation, thus eliminating special procedures required to generate semi-solid materials [12, 13]. Therefore, the semi-solid Mg-RE alloy prepared using isothermal heat treatment has been studied widely. SU et al [14] reported that to obtain an ideal semi-solid material, a suitable isothermal temperature and corresponding holding time for the Mg-Gd alloy were 630 °C and 30 min, respectively. HU et al [15] found that melting, which caused a reduction in α-Mg particle size, was the dominant mechanism in the initial stage whereas coalescence and Ostwald ripening tended to be subsequent principles in the evolution of semi-solid microstructures. Although previous studies have found that Mg atoms can be rearranged to form spherical grains during isothermal heat treatment [8], the evolution of RE-rich phases during semi-solid isothermal heat treatment is still poorly understood.

In recent years, researchers have expressed increasing interest in the advantageous microalloying effects of Mg-Gd-Al-Zn alloys, which exhibit better mechanical behavior compared to AZ (Mg-Al-Zn) and GZ (Mg-Gd-Zn) alloys [16−18]. Published literatures have revealed that the gadolinium can trigger the magnificent grain refinement via yielding of (Mg, Al)$_3$Gd and Al$_2$Gd phases in Mg-2Al-1Zn-*x*Gd alloys and thereby improving their high-temperature tensile properties [19]. Moreover, Gd-rich phases in Mg-Gd-Al-Zn alloys can suppress the formation of β-Mg$_{17}$Al$_{12}$ phases and promote heterogeneous nucleation, effectively improving the corrosion-resistant and heat-resistant properties of these alloys [20, 21]. Nevertheless, POURBAHARI et al [22] suggested that the branched (Mg,Al)$_3$Gd intermetallic compound would induce microvoid initiation sites and stress risers and therefore deteriorate tensile properties of the extruded Mg-4Gd-2Al-1Zn and Mg-2Gd-4Al- 1Zn alloys. However, discussions about whether these detrimental (Mg,Al)$_3$Gd phases can transform into Al$_2$Gd particles by heat treatment remain limited. Therefore, in the present work, considering that the Mg-Gd-Al-Zn alloy is a promising system of magnesium alloys, the microstructural evolution of as-cast and semi-solid AZ31-*x*Gd alloys is systematic investigated with a focus on the evolution of Gd-rich phases during isothermal heat treatment.

2 Experimental procedures

Commercial AZ31 and Mg-20%Gd (in wt.%) intermediate alloys were used to prepare the AZ31-*x*Gd alloys under a protective atmosphere of flowing CO_2 and SF_6 in a graphite crucible-resistant furnace. The required mass fraction Mg-20%Gd (in wt.%) intermediate alloys were added to the molten AZ31 alloy at 740 °C. Then, melts were held at 700 °C for 10 min to homogenize alloying elements before being poured into metallic molds which had been preheated to 200 °C with dimensions of Φ20 mm×150 mm. The chemical compositions of the as-cast AZ31-*x*Gd (*x*=0, 1.5 wt.%, 2.0 wt.% and 2.5 wt.%) alloys were analyzed by inductively coupled plasma-atomic emission spectrometry with results listed in Table 1. Before underwent isothermal heat treatment, the as-cast alloy ingots were cut into cylindrical samples with 15 mm in length and 20 mm in diameter.

Table 1 Chemical compositions of AZ31-*x*Gd (*x*=0, 1.5 wt.%, 2.0 wt.% and 2.5 wt.%) magnesium alloys (wt.%)

Alloy	Al	Zn	Mn	Gd	Mg
AZ31	2.64	0.96	0.33	−	Bal.
AZ31-1.5Gd	2.55	0.95	0.42	1.58	Bal.
AZ31-2.0Gd	2.59	1.05	0.36	2.03	Bal.
AZ31-2.5Gd	2.61	1.06	0.32	2.55	Bal.

Since the solidus and liquidus of AZ31 alloy are 566 and 627 °C, respectively, the temperatures of 585, 595, 605 and 615 °C were selected for isothermal heat treatment experiments. The

isothermal heat treatment was carried out in an electric-resistant furnace under a protective atmosphere of flowing CO_2 and SF_6. Samples with different compositions were heated to 585, 595, 605 and 615 °C and held for 5, 15, 30 and 45 min, respectively. Subsequently, samples were quenched promptly with cold water. The schematic diagram of essential experimental procedures is shown in Figure 1. The specimens were sectioned from the same position of semi-solid samples and prepared according to standard metallographic procedures. The etching solution was composed of 25 mL of ethanol, 1 g of picric acid, 1 mL of acetic acid, and 2 mL of distilled water. Another thin-foil specimen for TEM observation was sliced from semi-solid AZ31-2.0Gd alloy treated at 605 °C for 30 min and was mechanically polished to approximately 70-μm thickness; then, ion beam thinning was used to ensure that the thickness met TEM observation requirements. The microstructure characterization of the specimens was observed using optical microscopy (OM, Nican M200). Phase constituents were determined by X-ray diffraction (XRD, D8 ADVANCE) using Cu K_α radiation with a scanning angle (2θ) from 20° to 80° at a scanning rate of 5°/min. A scanning electron microscope (SEM; TESCAN VEGA 3) equipped with energy dispersive spectroscope (EDS) and a transmission electron microscope (TEM, JEM-2100) equipped with selected area electron diffraction (SAED) analysis were used to observe Gd-rich phases of AZ31-xGd alloys. Compression tests were carried out at room temperature using a Zwick universal material testing machine at a strain rate of 1×10^{-3} s^{-1}. Three cylindrical compressive specimens with the dimensions of Φ8 mm×12 mm were tested for each as-cast and semi-solid sample. Vickers hardness of the specimens is measured with a multifunctional microhardness tester (FISCHERSCOPE HM2000) under a load of 100 mN. The hardness measurements of isothermal heat treatment samples were tested at ten different solid-phase and liquid-phase regions respectively to obtain the arithmetic average value.

3 Results

3.1 Microstructural characterization

The XRD patterns of the as-cast AZ31 alloy (Alloy A), as-cast AZ31-2.0 wt.%Gd alloy (Alloy B), and semi-solid AZ31-2.0wt.%Gd alloy treated at 605 °C for 30 min (Alloy C) are shown in Figure 2. The spectrum of Alloy A indicates that the as-cast AZ31 alloy was composed of only α-Mg matrix and $Mg_{17}Al_{12}$ phases. However, the peaks of the $Mg_{17}Al_{12}$ phases disappeared whereas extra peaks of the Al_2Gd phase and $(Mg,Al)_3Gd$ phase were observed in the spectra of alloys B and C. According to Pauling electronegativity [23], the electronegativity difference between Al and Gd was larger than that between Al and Mg (Mg: 1.31; Al: 1.61; Gd: 1.2). Therefore, aluminum will preferentially react with gadolinium to form Al-Gd or Mg-Al-Gd phases instead of the $Mg_{17}Al_{12}$ phases in the Gd-modified AZ31 alloy. These Gd-rich phases were also mentioned by

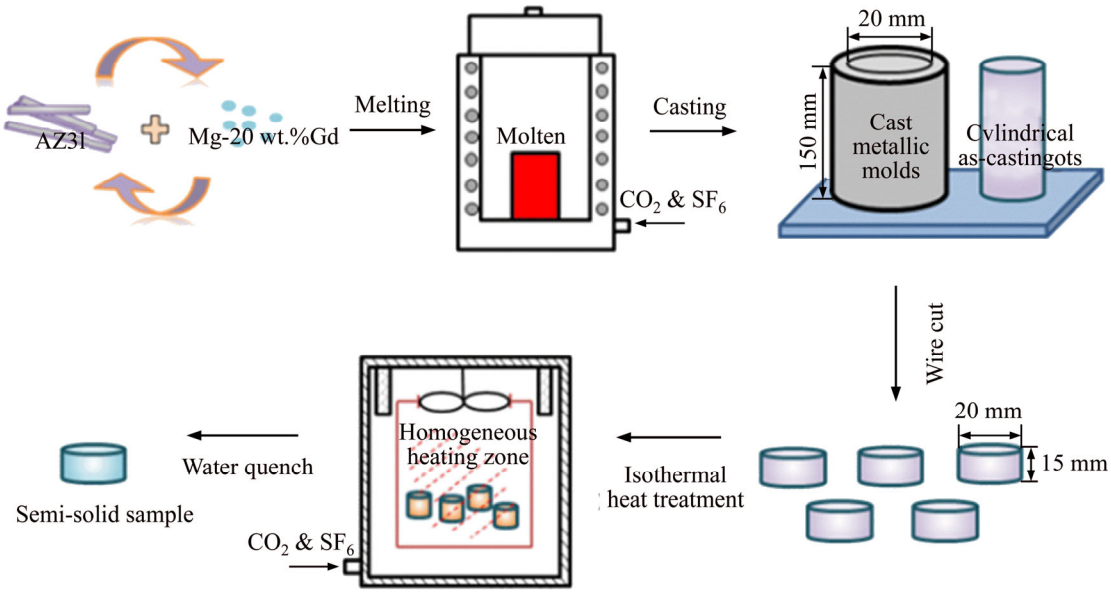

Figure 1 Schematic diagram of sample preparation process

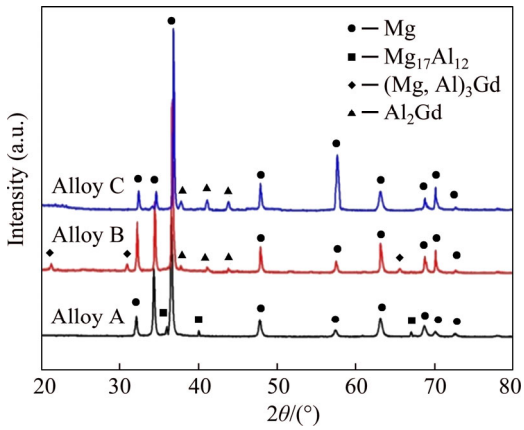

Figure 2 XRD patterns of Alloy A (as-cast AZ31), Alloy B (as-cast AZ31-2.0Gd), and Alloy C (semi-solid AZ31-2.0Gd treated at 605 °C for 30 min)

POURBAHARI et al [24]; they reported that when the Gd/Al atomic ratio exceeded 0.5, Al_2Gd phases and ternary $(Mg,Al)_3Gd$ phases would yield in the alloys. Following isothermal heat treatment, the peaks of the $(Mg,Al)_3Gd$ phase disappeared, implying that $(Mg,Al)_3Gd$ phases were not stable and decomposed at elevated temperature. Moreover, the increase of peak intensity at approximately 38°, 41.5°, and 44° demonstrated an increment of Al_2Gd phase.

Figure 3 presents SEM images captured by secondary electron (SE) mode and EDS analysis results of alloys A, B, and C. As shown in Figures 3(a) and (b), the as-cast AZ31 alloy mainly consisted of α-Mg and $Mg_{17}Al_{12}$ phases. Based on the XRD and EDS results, the addition of Gd led to the formation of angular particles (Point 1) and a lamellar-like phase (Point 2), deemed as Al_2Gd and $(Mg,Al)_3Gd$ phases, respectively, as shown in Figures 3(c), (d), (g) and (h). Following isothermal heat treatment (Figure 3(e)), fine and spherical grains with an average diameter of ~166 μm were obtained in the alloy. Nearly all $(Mg,Al)_3Gd$ phases disappeared during isothermal heat treatment, and a few of Al_2Gd particles distributed at interior of α-Mg grains while the others were enriched at the edges of spherical grains. These results suggest that the $(Mg,Al)_3Gd$ phases were unstable and decomposed, but Al_2Gd particles were thermally stable and survived during isothermal heat treatment, which is in line with the XRD analysis. When samples were quenched with cold water, the liquid phase cooled rapidly and formed fine primary and secondary dendrites composed mainly of Mg and partially dissolved Al (Point 3) (Figures 3(f) and (i)).

Figure 4 illustrates SEM-EDS elemental mapping of Gd-rich phases in Alloy C. It can be seen that many Al elements are enriched in the liquid phase while depleted in the solid phase. Additionally, the white angular particles around the α-Mg grains were mainly composed of Al and Gd elements. Figure 5 shows TEM images and corresponding selected area diffraction patterns (SAED) patterns along $[\bar{1}\,1\,2]$ zone axis of Gd-rich phase. Results indicate that this black phase inside the alloy has a face-centered cubic structure with measured lattice parameters of a=0.7890 nm, which is in accordance with Al_2Gd phase (a=0.7899 nm). The Al_2Gd and $(Mg,Al)_3Gd$ phases were also characterized based on TEM analysis by WANG et al [19].

3.2 Semi-solid microstructural evolution

The semi-solid microstructures of the AZ31-2.0Gd alloy treated at different temperatures for 30 min are presented in Figure 6. As shown in Figure 6(a), the dendritic morphology of the alloy evolved into irregular polygonal grains with some sharp corners after being held for 30 min at 585 °C. The eutectic mixtures distributed at the grain boundaries remelted first, while the liquid phase was relatively small due to the lower temperature. As the isothermal temperature increased to 595 °C, the α-Mg grains began to be uniformly refined and spheroidized, and some "liquid entrapment structure" formed at the interior of solid phases. The liquid phase increased and distributed continuously at the grain boundary, as depicted in Figure 6(b). When the isothermal temperature reached 605 °C (Figure 6(c)), the microstructure of the alloy modified by 2.0 wt.% Gd eventually evolved into fine near-spherical grains, and the volume fraction of the liquid phase far exceeded that of the alloy treated at 585 °C. When the temperature increased to 615 °C, however, the grain spherical effect declined substantially, and the superabundant liquid phases would yield dendrite-like morphology when the samples were treated by the quenching process in cold water, as indicated in Figure 6(d); that is, when the isothermal temperature was 615 °C or higher, the sample was not suitable for subsequent thixoforming.

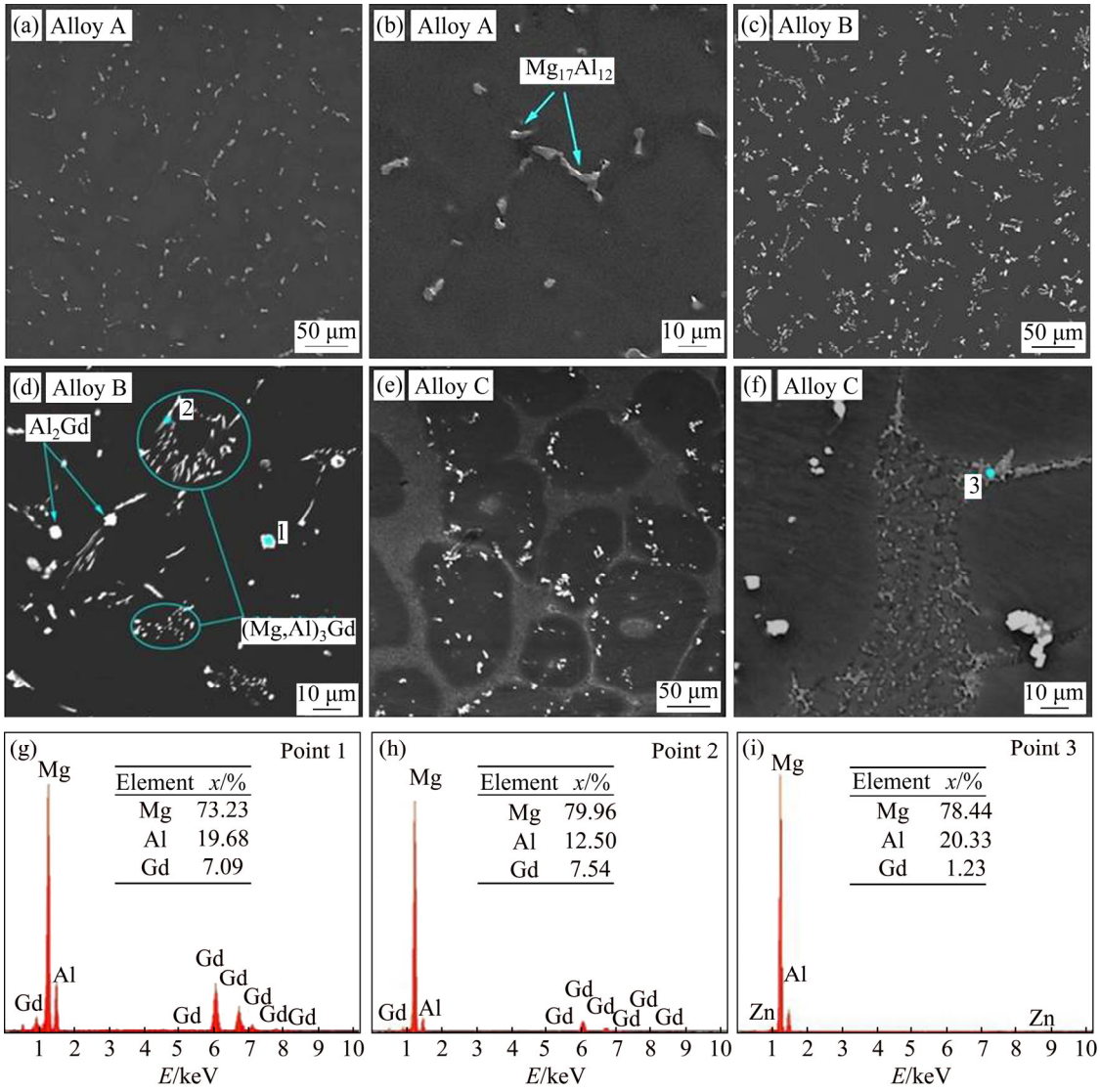

Figure 3 SEM images and EDS analysis of alloys A, B, and C: (a) Low-magnification SE image of Alloy A; (b) High-magnification SE image of Alloy A; (c) Low-magnification SE image of Alloy B; (d) High-magnification SE image of Alloy B; (e) Low-magnification SE image of Alloy C; (f) High-magnification SE image of Alloy C; (g) EDS at Area 1; (h) EDS at Area 2; (i) EDS at Area 3

Figure 7 displays the semi-solid microstructure of the AZ31-2.0Gd alloys held for various dwelling time at 605 °C. Figure 7(a) reveals that the dendritic morphology was replaced by large massive α-Mg grains after being held for 5 min and the liquid phase was discontinuously distributed at the grain boundary. At a dwelling time of 15 min (Figure 7(b)), the α-Mg grains were refined and round. The liquid phase began increasing, and some "liquid entrapment structure" formed inside the solid phases. After being held for 30 min at 605 °C, the α-Mg grains became finer and more rounded while the liquid phase increased substantially, as shown in Figure 7(c). However, the α-Mg grains became coarser as the dwelling time was prolonged up to 45 min (Figure 7(d)). The mechanisms about coarsening phenomenon of α-Mg grains will be deeply discussed in Section 4.2.

Figure 8 presents the effect of Gd content on semi-solid microstructures of AZ31-xGd (x=0, 1.5 wt.%, 2.0 wt.%, 2.5 wt.%) alloys held at 605 °C for 30 min dwell time. With increasing Gd content, the α-Mg grains changed from large massive-like shapes to fine spherical-like shapes. When the mass fraction of Gd in the alloy reached 2.0%, the grain size reached the minimum as shown in Figure 8(c). Figure 9 shows the statistical grain diameter and aspect ratio obtained by measuring 50 grains of the AZ31-xGd (x=0, 1.5 wt.%, 2.0 wt.%, 2.5 wt.%) alloys using the ImageJ image analyzer. The value

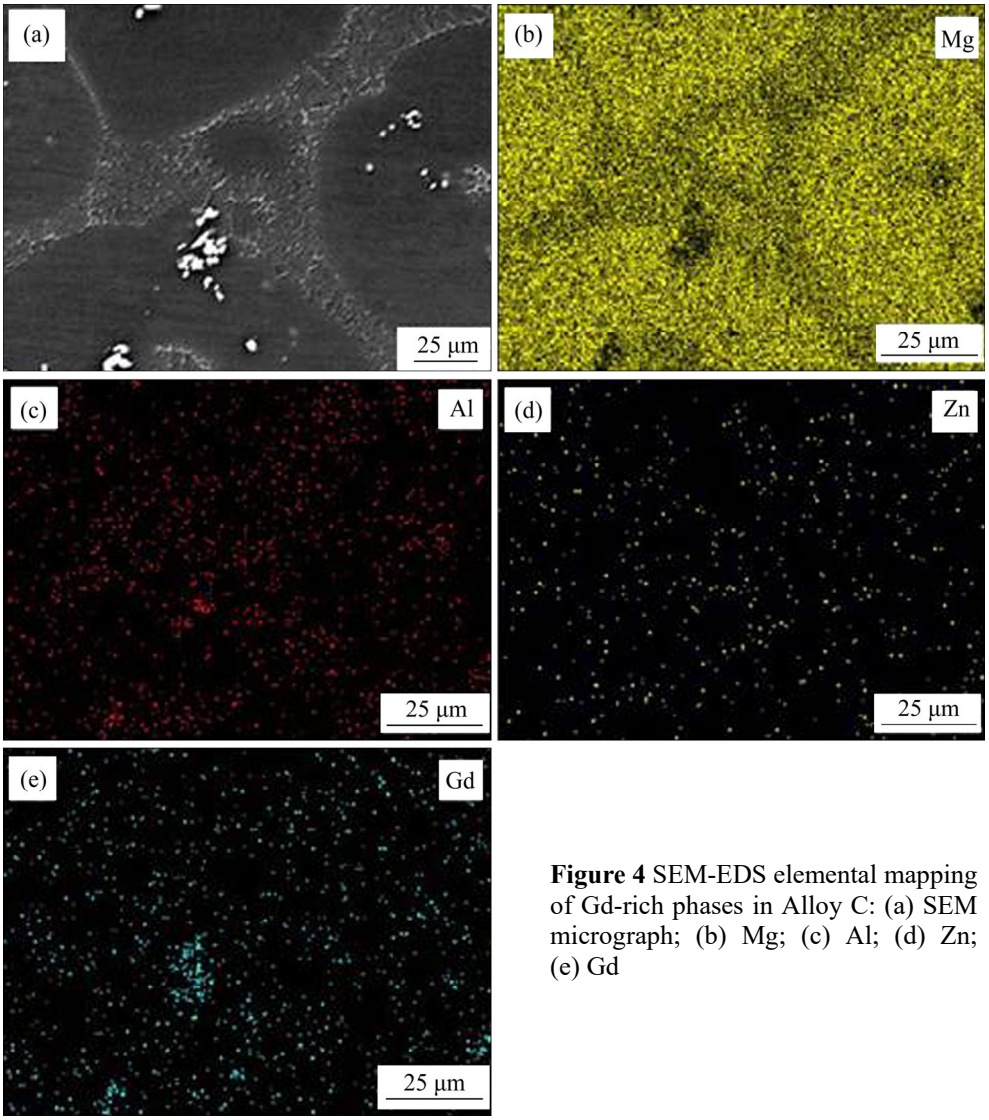

Figure 4 SEM-EDS elemental mapping of Gd-rich phases in Alloy C: (a) SEM micrograph; (b) Mg; (c) Al; (d) Zn; (e) Gd

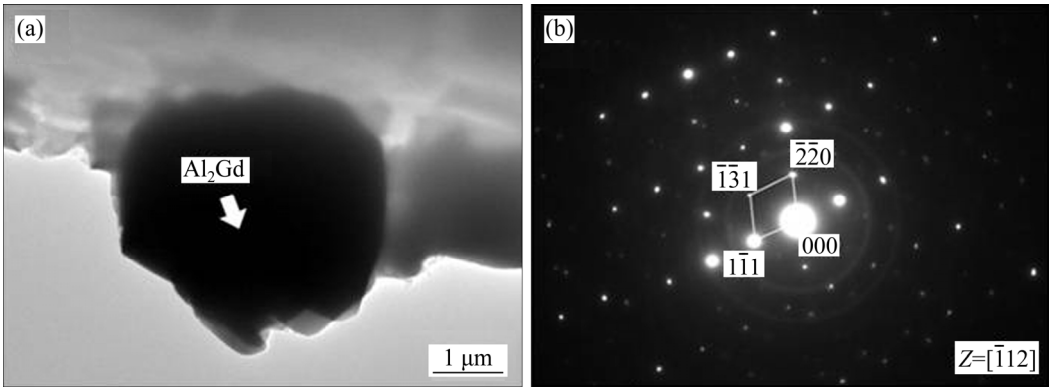

Figure 5 TEM images of Al_2Gd phase in Alloy C: (a) TEM image; (b) Corresponding SAED pattern

of the average grain diameter fell from 280 μm of the matrix alloy to 175 μm of the alloy modified with 2.0 wt.% Gd, and the corresponding aspect ratio had a slight reduction from 1.30 to 1.26. However, the grain size became larger when Gd content exceeded a certain value, primarily ascribed to the segregation of Al_2Gd phases at the solid-liquid interface, leading to the degradation in the supercooling effect of the Al_2Gd phases.

3.3 Mechanical properties

Published literatures have investigated the

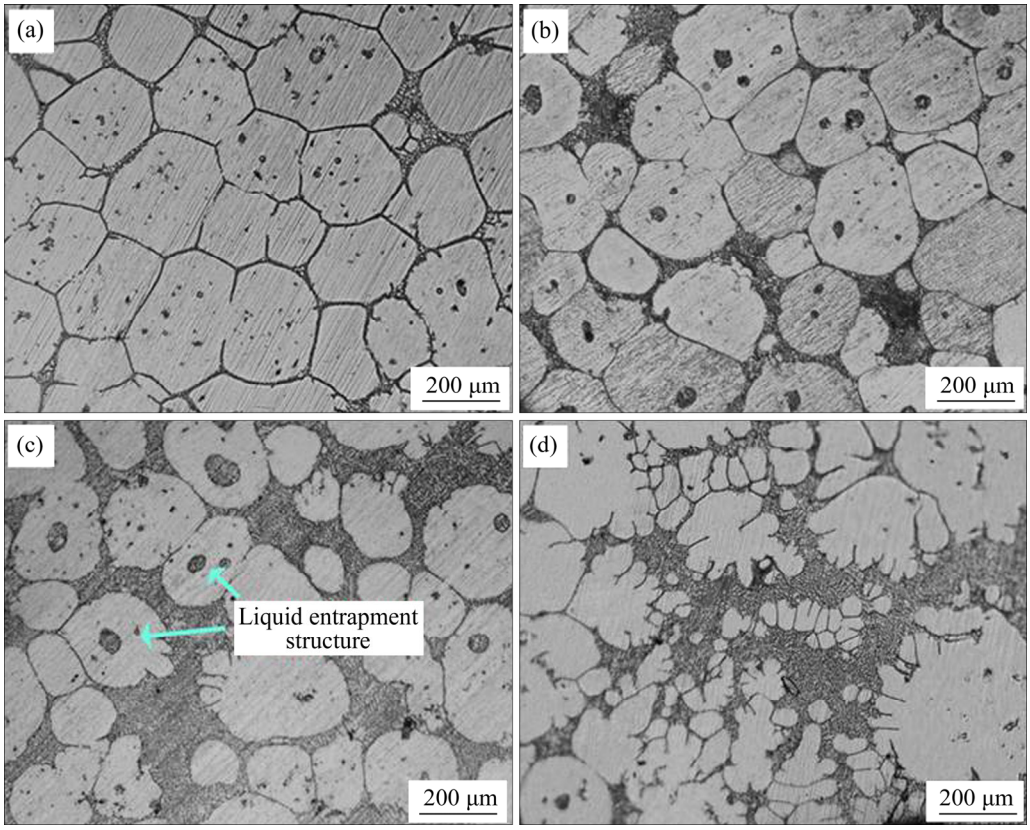

Figure 6 Semi-solid microstructure of AZ31-2.0Gd alloy treated at different isothermal temperatures for 30 min: (a) 585 °C; (b) 595 °C; (c) 605 °C; (d) 615 °C

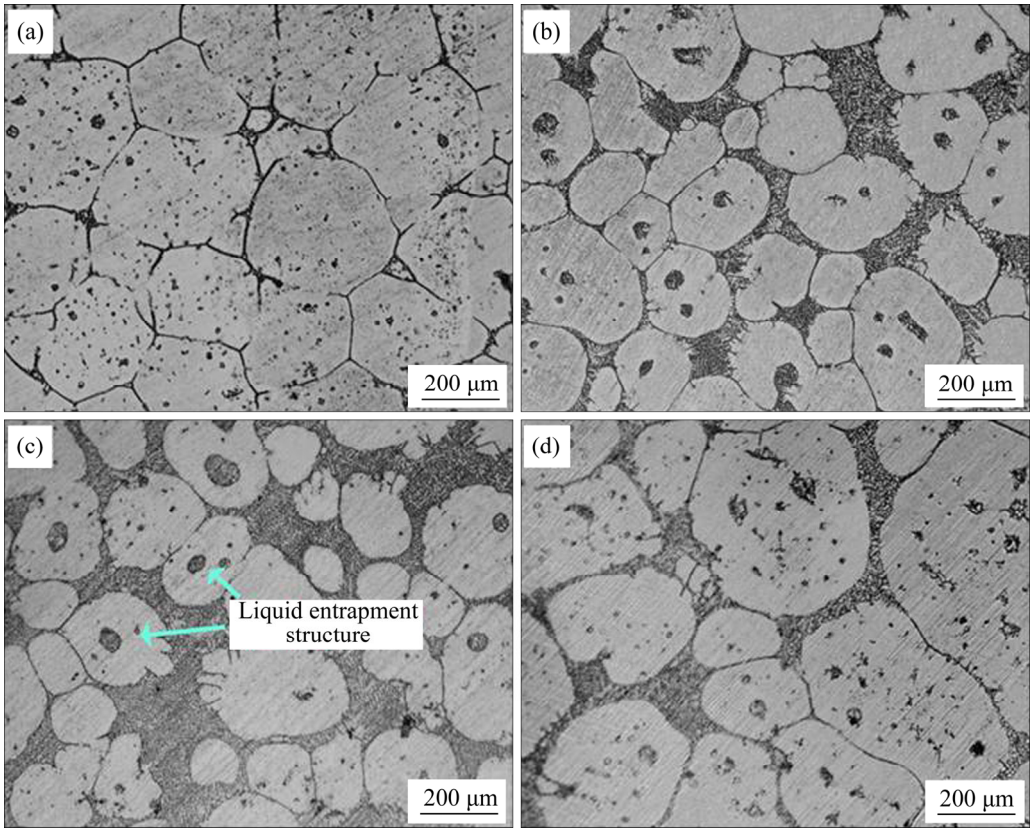

Figure 7 Semi-solid microstructure of AZ31-2.0Gd alloy treated at 605 °C for various dwelling times: (a) 5 min; (b) 15 min; (c) 30 min; (d) 45 min

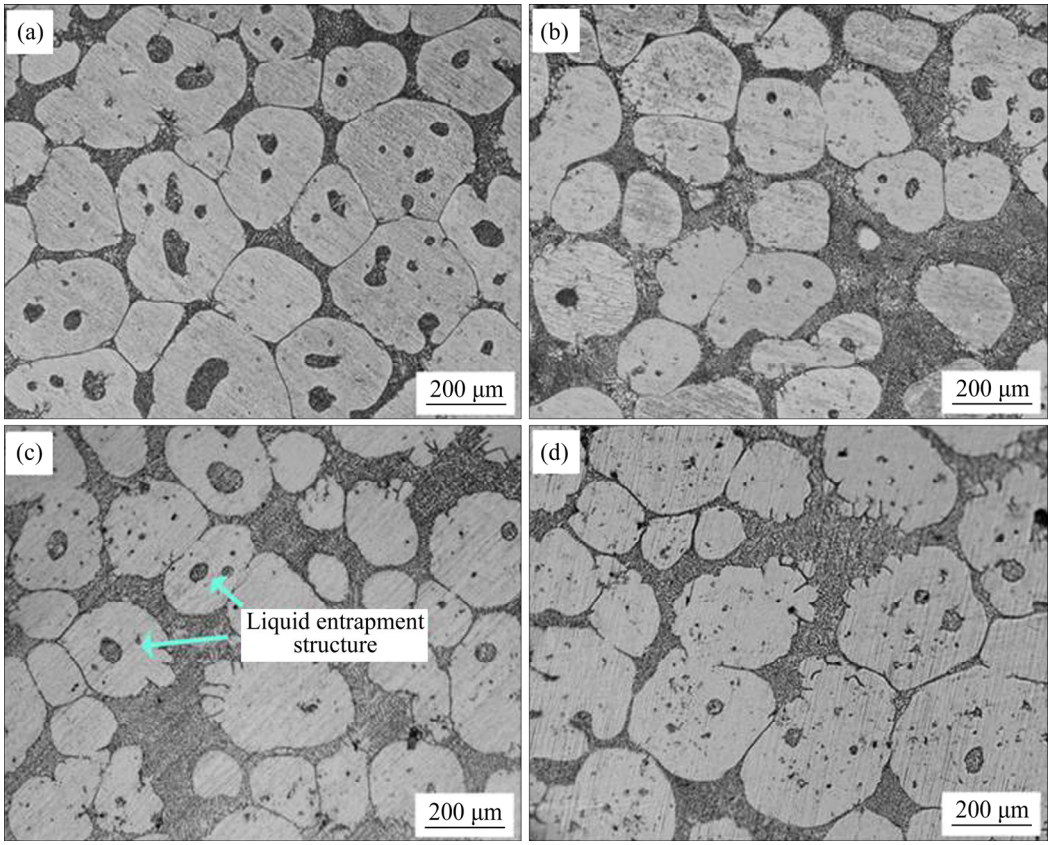

Figure 8 Semi-solid microstructure of AZ31 alloy treated at 605 °C for 30 min with different Gd contents: (a) 0 wt.%; (b) 1.5 wt.%; (c) 2.0 wt.%; (d) 2.5 wt.%

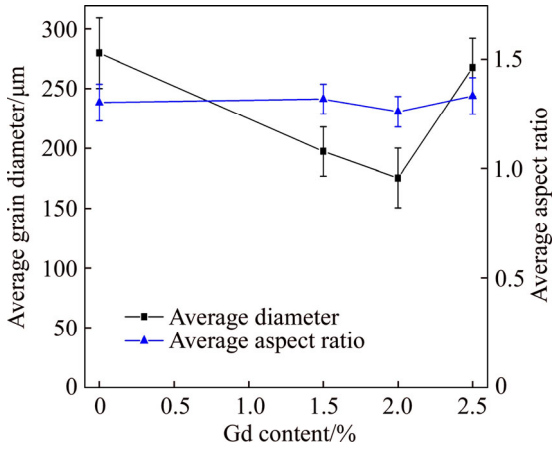

Figure 9 Average grain diameter and aspect ratio with change in Gd content at 605 °C for 30 min

effects of Gd on mechanical properties of as-cast AZ31 magnesium alloy and results showed that the hardness of AZ31 alloy was improved with the increasing of Gd content [25]. Thus, the current work mainly focuses on the hardness of AZ31-*x*Gd in semi-solid state. Figure 10 shows the microhardness of AZ31 and AZ31-2.0Gd alloy treaded by isothermal heat treatment at 605 °C for 30 min. As can be seen from the Figure 10(a), the average hardnesses of the solid phase and liquid phase in semi-solid AZ31 alloy were HV73 and HV60, respectively, whereas those values in semi-solid AZ31-2.0Gd alloy were HV80 and HV60, respectively. It was worth mentioning that the value was as high as HV84 at the edge of solid phase (enriched Al_2Gd region) in semi-solid AZ31-2.0Gd alloy (Figure 10(b)). From the above results, it can be concluded that the hardness of the solid phase was much higher than that of the liquid phase, and the overall hardness of semi-solid AZ31-2.0Gd alloy was improved in comparison with the semi-solid AZ31 alloy due to the Gd addition. Meanwhile, the tone-up effect was more obvious in the place where the Al_2Gd phase was enriched.

The representative compression engineering stress−strain curve of as-cast AZ31, semi-solid AZ31 at 605 °C for 30 min and semi-solid AZ31-2.0Gd alloy at 605 °C for 30 min at room temperatures are shown in Figure 11. It can be seen that the compressive strength (σ_{max}) values of as-cast AZ31, semi-solid AZ31 and semi-solid AZ31-2.0Gd are 280, 209 and 230 MPa, respectively. Note that the σ_{max} of the semi-solid

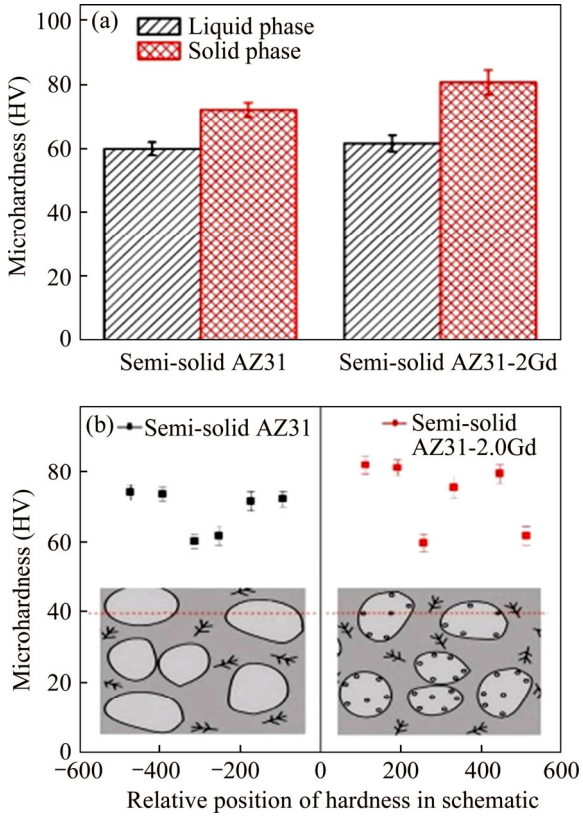

Figure 10 Microhardness of AZ31 and AZ31-2.0Gd alloy treaded by isothermal heat treatment at 605 °C for 30 min: (a) Average microhardness of liquid phase and solid phase; (b) Microhardness distribution along red dashed line

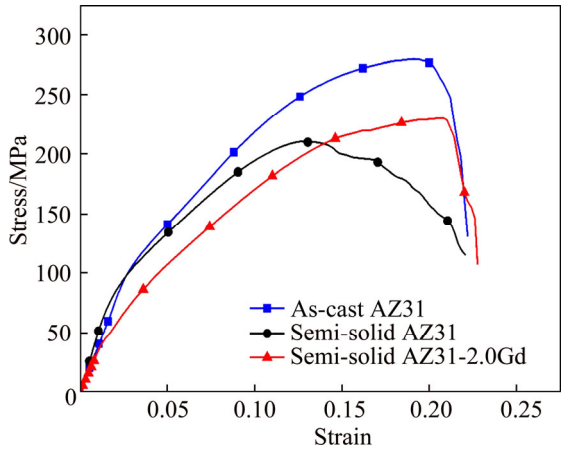

Figure 11 Representative compression engineering stress−strain curve of as-cast AZ31, semi-solid AZ31 at 605 °C for 30 min and semi-solid AZ31-2.0Gd alloy at 605 °C for 30 min

samples is lower than that of the as-cast one, indicating that a reduction of compressive deformation resistance has been successfully achieved after semi-solid isothermal heat treatment. In the present work, the semi-solid samples consisted of fine non-dendritic grains and a large amount of liquid phase. This means that the required load for semi-solid grains to deform will be much lower than that for as-cast individual dendritic to deform, because applied load of the former mainly needs to overcome the frictional force caused by the relative motion between spherical grains [26]. However, the compression deformation behavior of dendritic structure alloys includes not only dislocation and slip interaction but also the fragmentation of the dendritic structure [27]. In addition, the liquid phase in the semi-solid samples plays a role as a lubricant to relax the stress concentrations [28]. Therefore, it is plausible to observe a superior formability in semi-solid AZ31 than the as-cast one. After introducing gadolinium into the AZ31, the σ_{max} of the semi-solid AZ31-2.0Gd alloy is improved in comparison with that of semi-solid AZ31, but still lower than that of the as-cast one. The increment of strength in Gd-containing semi-solid AZ31 alloy is mainly attributed to the formation of the Al_2Gd phases. A few of the Al_2Gd particles acted as the grain refining inoculant in dynamic remelting-solidification equilibrium procession, while more Al_2Gd particles located at solid-liquid interface can hinder the growth of Mg grains during isothermal heat treatment, resulting in a grain refinement effect. Meanwhile, the Al_2Gd particles distributed inside the grains can exert intense retardation for dislocation movements (Orowan-type). It was worth pointing out that we only compared the deformability of semi-solid billets for the die-forging forming here, while the mechanical properties of the final part could be much better under the synergy of grain refinement and Orowan strengthening induced by Al_2Gd particles, which is the focus of our future research.

4 Discussion

4.1 Evolution of Gd-rich phases during isothermal heat treatment

Most Al_2Gd particles were distributed around the edge of the spherical α-Mg grains in semi-solid AZ31-2.0%Gd, as shown in Figures 3(e) and (f). This phenomenon was also observed in semi-solid AZ61-xSm magnesium alloys, mainly attributed to the forces acting on Al_2Sm particles in front of the solid-liquid interface, leading to the accumulation

of Al_2Sm particles at the interface [29]. The XRD and SEM analysis results show that the lamellar structure $(Mg,Al)_3Gd$ phase in the AZ31-2.0Gd alloy disappeared and more particle-like Al_2Gd formed after heat treatment. A schematic diagram of the phase transformation between $(Mg,Al)_3Gd$ and Al_2Gd phases in as-cast AZ31-xGd alloys during isothermal heat treatment is shown in Figure 12.

As indicated in Figure 12(a), the regions like "A" in the lamellar-like $(Mg,Al)_3Gd$ phase exhibited a relatively small curvature radius. According to the Gibbs-Thomson formula, the Gd concentration corresponds to the site where the $(Mg,Al)_3Gd$ phase has a smaller curvature radius, expressed as [30]:

$$C_{Gd}(r)=C_{Gd}(\infty)\exp\left(\frac{2\sigma v_B}{k_B T r}\right) \quad (1)$$

where $C_{Gd}(r)$ is the Gd concentration at the position with a curvature radius, r; $C_{Gd}(\infty)$ is the Gd concentration at the flat interface; σ is the surface tension; v_B is the volume of the Gd atom; T is the temperature; and k_B is the coefficient related to the shape. As per Eq. (1), the smaller the curvature radius is, the higher the Gd concentration is. Therefore, during isothermal heat treatment, Gd atoms diffused from the position where Gd atom concentration was high to the position where the concentration was lower. As a result, the diffusion interactions of Gd atoms promoted positions with smaller curvature radius to exhibit "necks" and detach from parent phase, as depicted in Figure 12(b). When temperature reached a certain value, transformation occurred between cracked $(Mg,Al)_3Gd$ and Al_2Gd phase, expressed as

$$(Mg,Al)_3Gd \rightarrow Al_2Gd+Mg \quad (2)$$

This transformation was promoted by a set of matching parameters (orientation relationship) between the $(Mg,Al)_3Gd$ and Al_2Gd phases. A similar scenario appeared in the transformation between pyrochlore and spinel [31]. Figure 12(c) demonstrates that new Al_2Gd phases nucleated within $(Mg,Al)_3Gd$ phases in these similar orientation relationships. Finally, the newly formed Al_2Gd phases were distributed in the corresponding areas, as shown in Figure 12(d) and Figure 3(e).

4.2 Microstructural evolution of as-cast AZ31-xGd alloys during isothermal heat treatment

In the present study, the grain refinement of semi-solid microstructures due to Gd additions was discussed; a schematic diagram of the microstructural evolution of as-cast AZ31-xGd alloys during isothermal heat treatment is shown in Figure 13. The microstructure of the as-cast alloy showed a primary equiaxed dendrites with some

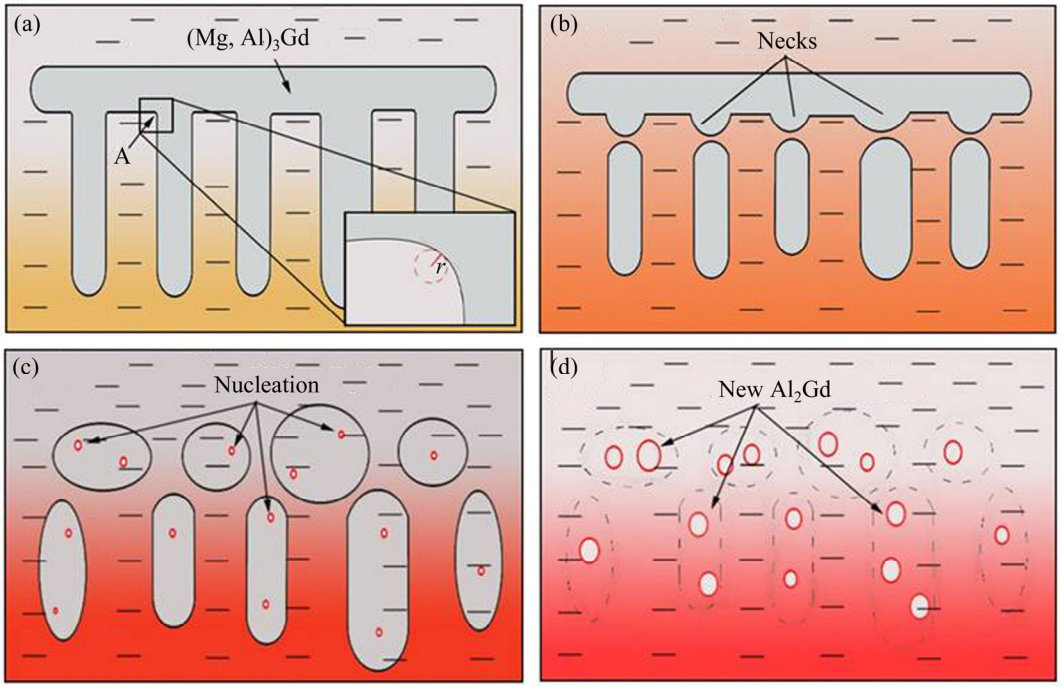

Figure 12 Schematic diagram of $(Mg,Al)_3Gd$ phase transformation in as-cast AZ31-xGd alloys during semi-solid isothermal heat treatment

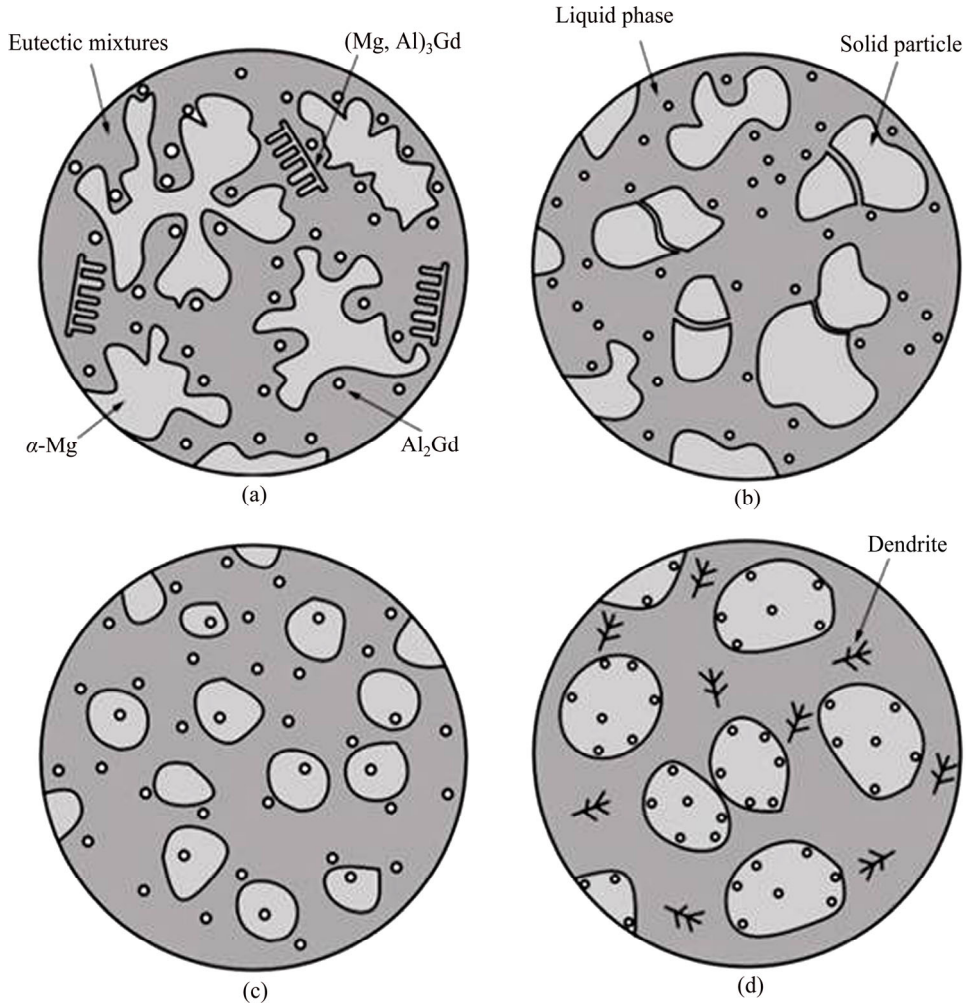

Figure 13 Schematic diagram of microstructural evolution of as-cast AZ31-*x*Gd alloys during isothermal heat treatment: (a) Equiaxed dendrites; (b) Remelting; (c) Dynamic balance; (d) Rapid cooling

Al_2Gd and $(Mg,Al)_3Gd$ secondary phase, as indicated in Figures 13(a) and (c). The angular Al_2Gd particles and lamellar-like $(Mg,Al)_3Gd$ phases were mainly distributed within grain boundaries, which could mechanically hinder the growth of α-Mg dendrites during solidification. Previous investigation has shown that the finer the as-cast dendrites, the more small and spherical the grains after isothermally heat-treatment [32].

Once the temperature reached a certain value, $(Mg,Al)_3Gd$ phases transformed to Al_2Gd phases via the evolution process mentioned in Section 4.1. Meanwhile, the remelting of dendritic branches played a significant role in the non-dendritic morphology evolution, as shown in Figure 13(b). The remelting process is driven by the discrepancy of the equilibrium melting point caused by different curvature of the dendritic. Relationship between the equilibrium melting point and curvature of the dendritic interface is expressed as [15]:

$$\Delta T_r = -\frac{2\sigma T_m V_s k}{\Delta H_m} \quad (3)$$

where ΔT_r is the variation of equilibrium melting point at the solid-liquid interface with a curvature, k; T_m is the melting point of flat solid-liquid interface; σ is the surface tension; V_s is the volume of solid phase per molar; and ΔH_m is the enthalpy of liquid-solid transformation per molar. As per Eq. (3), the melting point will decrease at the larger curvature positions, which leads to circumflex areas having a priority to melt and yield narrow necks. Then, these frail necks are inclined to pinch-off from the parent stem to exhibit a fine and isotropic grains. Therefore, the remelting of dendritic branches is believed to be the main mechanism for the formation of non-dendritic morphology. Moreover, with the solid phases melting, the liquid entrapment structure can be observed in

non-dendritic microstructure, which is well described via 4D (3D + time) synchrotron tomography by GUO et al [33]. Through the three spatial dimensions evidence, it can be clearly seen that the "small liquid entrapment" inside the solid phase is a kind of grooves left by a large number of the dissolution of small branches. Additionally, particle spheroidization also occurred at this stage, creating rounder and more uniform grains [34].

For the next moment (Figure 13(c)), the solid-liquid phases achieved a balance state, indicating that the volume fraction of solid and liquid phases remained almost constant. It is worth noting that, however, the remelted solid phase formed new grains with a smaller size due to the refined effect of Al_2Gd particles (including those transformed from $(Mg,Al)_3Gd$ phases). Published literatures have proved that Al_2Gd particles can function as an ideal grain refining inoculant due to the small interatomic spacing misfit (f_r) and interplanar spacing mismatch (f_d) between Al_2Gd and α-Mg at orientation relationships of $<112>_{Al_2Gd}//<2\bar{1}\bar{1}0>_{\alpha\text{-Mg}}$, $\{4\bar{4}0\}_{Al_2Gd}//\{0\bar{1}10\}_{\alpha\text{-Mg}}$, $\{\bar{3}11\}_{Al_2Gd}//\{0\bar{1}11\}_{\alpha\text{-Mg}}$, where the maximum values of f_r and f_d were both smaller than 2.9% [35]. This value is far less than the most effective nucleation value of 6%; therefore, a small number of the Al_2Gd particles inside α-Mg grains (Figure 2(e)) provoke nucleation and lead to the formation of finer spherical grains during the period of remelting and solidification equilibrium, which could be the auxiliary factors of grain refinement.

Although a few of Al_2Gd particles acted as grain refining inoculants in the α-Mg grains, more Al_2Gd particles were enriched at the edge of spherical grains. According to the interface energy principle [36], solid grains can combine only when the interfacial energy γ_{ss} between the solid phases is less than the interfacial energy γ_{sl} between the solid and liquid phases. Due to a large amount of Al_2Gd particles at the edge of α-Mg grains, it is difficult to satisfy $\gamma_{ss}<\gamma_{sl}$ during short-time isothermal heat treatment, which remarkably enhanced the grain refinement effect. However, a long-time isothermal heat treatment will cause the interface size to increase and become unstable. As a result, the α-Mg grains will spontaneously become coarser to reduce the total interfacial energy with the increasing of the isothermal time, as shown in Figure 13(d) and Figure 7(d). This coarsening phenomenon is mainly caused by two mechanisms: 1) coalescence ripening and 2) Ostwald ripening. The first coarsening mechanism is a diffusion-controlled process and its rate will be determined by the value of diffusion coefficient, which has an exponential relationship with the temperature. To be specific, the equilibrium vacancy concentration would significantly boom with the increasing of temperature and holding time. Thus, the interdiffusion of Mg atoms between adjacent grains would easily take place at a relative high solid volume fraction [37]. When the dwelling time was long enough, Ostwald ripening mechanism played a major role at the lower solid volume fraction state, which acted via the growth of large particles and the dissolution of small particles [38]. Both of coalescence ripening and Ostwald ripening make the average size of α-Mg grains increase. Similar coarsening evolution in Ga-In alloy was also observed by HEYME et al [39]; They provided directly experimental evidence by real-time in-situ synchrotron technique and established an idealized phase-field model for microstructure evolution during isothermally heat-treatment. Following water quenching, many fine primary and secondary dendrites were yielded in the liquid phases and many Al_2Gd particles solidified at the edge of semi-solid spherical grains, (Figures 13(d) and (e)).

5 Conclusions

1) The microstructure of the as-cast AZ31-xGd alloy was composed of a dominant α-Mg matrix, lamellar $(Mg,Al)_3Gd$ phases, and Al_2Gd particles. During isothermal heat treatment, phase transformation occurred between the $(Mg,Al)_3Gd$ phases and Al_2Gd phases, resulting in the formation of particle-like Al_2Gd phases and the decomposition of $(Mg,Al)_3Gd$ phases.

2) When the Gd was added into the alloy, finer and more rounded α-Mg grains formed in AZ31 magnesium alloys during semi-solid isothermal heat treatment. When the mass fraction of Gd in the alloy reached 2.0%, the sizes of spherical grains reached the minimum.

3) The main mechanism of grain refinement lies in the remelting of dendritic branches as well as the auxiliary effect of a small number of Al_2Gd

particles as grain refining inoculants. Meanwhile, Al_2Gd particles enriched at the solid-liquid interfaces can remarkably retard the growth rate of α-Mg grains.

4) A reduction of deformation resistance has been successfully achieved in AZ31-2.0Gd magnesium alloy after semi-solid isothermal heat treatment, which shows a moderate compressive deformation resistance (230 MPa), comparing to the as-cast AZ31 (280 MPa) and semi-solid AZ31 (209 MPa). In addition, the microhardness of the solid phase was much higher than that of the liquid phase, and the overall hardness of semi-solid AZ31-2.0Gd alloy was improved in comparison with semi-solid AZ31 alloy. The grain refinement and the second phase strengthening induced by gadolinium are the main strengthening mechanism of semi-solid AZ31-2.0Gd magnesium alloy.

Contributors

CHU Chen-liang performed the data analyses and wrote the manuscript; YAN Hong and LUO Chao helped perform the analysis with constructive discussions; TANG Bin-bing helped with the TEM analysis; WU Xiao-quan and QIU Shui-cai played an important role in interpreting the results; YIN Zheng contributed significantly to manuscript preparation; HU Zhi contributed to the conception of the study.

Conflict of interest

These authors declare no conflict of interest.

References

[1] CHEN Gang, ZHANG Yan-bin, XIA Wei-jun, CHEN Ding. Microstructure and tensile creep resistance of Mg-5.5%Zn-(0.7%, 1.5%, 3.5%, 7.5%)Y alloys [J]. Journal of Central South University, 2015, 22: 4112−4122. DOI: 10.1007/s11771-015-2957-0.

[2] WU F, ZHANG S, TAO Z. Corrosion behavior of 3C magnesium alloys in simulated sweat solution [J]. Materials and Corrosion, 2011, 62(3): 234−239. DOI: 10.1002/maco.200905510.

[3] LIU Huan, HUANG He, SUN Jia-peng, WANG Ce, BAI Jing, MA Ai-bin, CHEN Xian-hua. Microstructure and mechanical properties of Mg–RE–TM cast alloys containing long period stacking ordered phases: A review [J]. Acta Metallurgica Sinica (English Letters), 2019, 32: 269−285. DOI: 10.1007/s40195-018-0862-x.

[4] GARCES G, PEREZ P, BAREA R, MEDINA J, STARK A, SCHELL N, ADEVA P. Increase in the mechanical strength of Mg-8Gd-3Y-1Zn alloy containing long-period stacking ordered phases using equal channel angular pressing processing [J]. Metals, 2019, 9: 221. DOI: 10.3390/met9020221.

[5] ZHANG Jing-huai, LIU Shu-juan, WU Rui-zhi, HOU Le-gan, ZHANG Mi-lin. Recent developments in high-strength Mg-RE-based alloys: Focusing on Mg-Gd and Mg-Y systems [J]. Journal of Magnesium and Alloys, 2018, 6: 277−291. https://doi.org/10.1016/j.jma.2018.08.001.

[6] LIU Huan, HUANG He, WANG Ce, SUN Jia-peng, BAI Jing, XUE Feng, MA Ai-bin, CHEN Xiao-bo. Recent advances in LPSO-containing wrought magnesium alloys: Relationships between processing, microstructure, and mechanical properties [J]. JOM, 2019, 71: 3314−3327. https://doi.org/10.1007/s11837-019-03610-9.

[7] CHEN Tian, XIE Zhi-wen, LUO Zhuang-zhu, YANG Qin, TAN Sheng, WANG Yun-jiao, LUO Yi-min. Microstructure evolution and tensile mechanical properties of thixoformed AZ61 magnesium alloy prepared by squeeze casting [J]. Transactions of Nonferrous Metals Society of China, 2014, 24: 3421−3428. DOI: 10.1016/S1003-6326(14)63485-3.

[8] JIANG Ju-fu, LIN Xin, WANG Ying, QU Jian-jun, LUO Shou-jing. Microstructural evolution of AZ61 magnesium alloy predeformed by ECAE during semisolid isothermal treatment [J]. Transactions of Nonferrous Metals Society of China, 2012, 22: 555−563. DOI: 10.1016/S1003-6326(11)61213-2.

[9] YANG Zhao, XU Hong-yu, WANG Ye, HU Mao-liang, JI Ze-sheng. Investigation of the microstructure and mechanical properties of AZ31/graphene composite fabricated by semi-solid isothermal treatment and hot extrusion [J]. JOM, 2019, 71: 4162−4170. DOI: 10.1007/s11837-019-03736-w.

[10] YAN Hong, ZHOU Bing-fen. Thixotropic deformation behavior of semi-solid AZ61 magnesium alloy during compression process [J]. Materials Science and Engineering B, 2006, 132: 179−182. DOI:10.1016/j.mseb.2006.02.020.

[11] WANG Cun-long, CHEN An-tao, ZHANG Liang, LIU Wen-cai, WU Guo-hua, DING Wen-jiang. Preparation of an Mg-Gd-Zn alloy semisolid slurry by low frequency electro-magnetic stirring [J]. Materials and Design, 2015, 84: 53−63. DOI: 10.1016/j.matdes.2015.06.126.

[12] WANG Hui-Yuan, ZHA Min, LIU Bo, WANG Dong-Ming, JIANG Qi-Chuan. Microstructural evolution behavior of Mg-5Si-1Al alloy modified with Sr-Sb during isothermal heat treatment [J]. Journal of Alloys and Compounds, 2009, 480: 25−28. DOI: 10.1016/j.jallcom.2009.02.044.

[13] XIAO Guan-fei, JIANG Ju-fu, LIU Ying-ze, WANG Ying, GUO Bao-yong. Recrystallization and microstructure evolution of hot extruded 7075 aluminum alloy during semi-solid isothermal treatment [J]. Materials Characterization, 2019, 156: 109874. DOI: 10.1016/j.matchar.2019.109874.

[14] SU Gui-hua, CAO Zhan-yi, LIU Yong-bing, WANG Yu-hui, ZHANG Liang, CHENG Li-ren. Effects of semi-solid isothermal process parameters on microstructure of Mg-Gd alloy [J]. Transactions of Nonferrous Metals Society of China, 2010, 20: 402−406.

[15] HU Yong, RAO Li, NI Xu-wu. Effect of isothermal heat treatment on semi-solid microstructure of AZ91D magnesium alloy containing rare earth Gd [J]. China Foundry, 2015, 12(1): 20−25.

[16] XIE Zhen-dong, GUAN Yan-jin, YU Xiao-hui, ZHU Li-hua, LIN Jun. Effects of ultrasonic vibration on performance and microstructure of AZ31 magnesium alloy under tensile deformation [J]. Journal of Central South University, 2018, 25: 1545−1559. DOI: 10.1007/s11771-018- 3847-z.

[17] POURBAHARI B, MIRZADEH H, EMAMY M, ROUMINA R. Enhanced ductility of a fine-grained Mg-Gd-Al-Zn magnesium alloy by hot extrusion [J]. Advanced Engineering Materials, 2018, 20: 1701171. DOI: 10.1002/adem.201701171.

[18] GUO Quan-ying, LIU Zheng, MAO Ping-li, SUN Jing. Effect of aging temperature on microstructure and mechanical properties of AZ81-4%Gd magnesium alloy. [J]. Materials Science Forum, 2013, 747−748: 301−306. DOI: 10.4028/www.scientific.net/MSF.747-748.301.

[19] WANG Xu-dong, DU Wen-bo, LIU Ke, WANG Zhao-hui, LI Shu-bo. Microstructure, tensile properties and creep behaviors of as-cast Mg-2Al-1Zn-*x*Gd (*x*=1, 2, 3 and 4wt.%) alloys [J]. Journal of Alloys and Compounds, 2012, 522: 78−84. DOI: 10.1016/j.jallcom.2012.01.084.

[20] ARRABAL R, MATYKINA E, PARDO A, MERINO M C, PAUCAR K, MOHEDANO M, CASAJÚS P. Corrosion behaviour of AZ91D and AM50 magnesium alloys with Nd and Gd additions in humid environments [J]. Corrosion Science, 2012, 55: 351−362. DOI: 10.1016/j.corsci.2011. 10.038.

[21] POURBAHARI B, MIRZADEH H, EMAMY M. Elucidating the effect of intermetallic compounds on the behavior of Mg-Gd-Al-Zn magnesium alloys at elevated temperatures [J]. Journal of Materials Research, 2017, 32(22): 4186−4195. DOI: 10.1557/jmr.2017.415.

[22] POURBAHARI B, MIRZADEH H, EMAMY M. The Effects of Grain refinement and rare earth intermetallics on mechanical properties of as-cast and wrought magnesium alloys [J]. Journal of Materials Engineering and Performance 2018, 27(3): 1327−1333. DOI: 10.1007/s11665-018-3238-5.

[23] LU Fu-min, MA Ai-bin, JIANG Jing-hua, GUO Yu, YANG Dong-hui, SONG Dan, CHEN Jian-qing. Significantly improved corrosion resistance of heat-treated Mg-Al-Gd alloy containing profuse needle-like precipitates within grains [J]. Corrosion Science, 2015, 94: 171−178. http://dx.doi.org/10.1016/j.corsci.2015.01.052.

[24] POURBAHARI B, EMAMY M, MIRZADEH H. Synergistic effect of Al and Gd on enhancement of mechanical properties of magnesium alloys [J]. Progress in Natural Science: Materials International, 2017, 27: 228−235. DOI: 10.1016/ j.pnsc.2017.02.004.

[25] SONG Ting-yu, WANG Wen-chuan, YANG Xiao-yu, MAO Hong-kui, XU Hong. Influence of Gd content on microstructure and mechanical properties of AZ31 alloy [J]. Foundry Technology, 2015, 36(5): 1208−1210. DOI: 10.16410/j.issn1000-8365.2015.05.038. (in Chinese)

[26] YANG H L, ZHANG Z L, OHNAKA I. Structure evolution and compressive behavior of semi-solid Al–Si hypoeutectic alloy with re-melting heat treatment [J]. Journal of Materials Processing Technology, 2004, 151: 155−164. DOI: 10.1016/j.jmatprotec.2004.04.031.

[27] YANG M B, HU H J, DAI B, TANG L W. Compression behaviour of semisolid YL112 die casting aluminium alloy following isothermal heat treatment [J]. International Journal of Cast Metals Research, 2007, 20(4): 198−201. DOI: 10.1179/136404607X249770.

[28] CHINO Y, KOBATA M, IWASAKI H, MABUCHI M. An investigation of compressive deformation behaviour for AZ91 Mg alloy containing a small volume of liquid [J]. Acta Materialia, 2003, 51: 3309−3318. DOI: 10.1016/S1359-6454(03)00162-9.

[29] CHU Chen-liang, HU Zhi, LI Xiao, YAN Hong, WU Xiao-quan, MAI Yuan-lu. Evolution and distribution of Al_2Sm phase in as-extruded AZ61-*x*Sm magnesium alloys during semi-solid isothermal heat-treatment [J]. Transactions of Nonferrous Metals Society of China, 2018, 28: 1311−1320. DOI: 10.1016/S1003-6326(18)64768-5.

[30] NISHIOKA K, MAKSIMOV I L. Reconsideration of the concept of critical nucleus and the Gibbs-Thomson equation [J]. Journal of Crystal Growth, 1996, 163: 1−7. DOI: 10.1016/0022-0248(95)01033-5.

[31] WONG J. Microstructure and phase transformation in a highly non-Ohmic metal oxide varistor ceramic [J]. Journal of Applied Physics, 1975, 46: 1653−1659. DOI: 10.1063/1.321768.

[32] CHEN T J, HAO Y, SUN J, LI Y D. Effects of Mg and RE additions on the semi-solid microstructure of a zinc alloy ZA27 [J]. Science and Technology of Advanced Materials, 2003, 4: 495−502. DOI: 10.1016/j.stam.2004.01.002.

[33] GUO En-yu , PHILLION A B, CAI Biao, SHUAI San-san, KAZANTSEV D, JING Tao, LEE P D. Dendritic evolution during coarsening of Mg-Zn alloys via 4D synchrotron tomography [J]. Acta Materialia, 2017, 123: 373−382. http://dx.doi.org/10.1016/j.actamat.2016.10.022.

[34] TAO Jian-quan, JI Xing-hua, ZHANG Yan-ping, SUN Chang-jian, DENG Tian-quan. Microstructure evolution of Mg-Gd-Y-Zn-Zr magnesium alloy during partial remelting [J]. Materials Science−Medziagotyra, 2014, 20(4): 436−439. http://dx.doi.org/10.5755/j01.ms.20.4.6483.

[35] DAI Ji-chun, EASTON M, ZHU Su-ming, WU Guo-hua, DING Wen-jiang. Grain refinement of Mg-10Gd alloy by Al additions [J]. Journal of Materials Research, 2012, 27: 2790−2797. DOI: 10.1557/jmr.2012.313.

[36] LOUÉ W R, SUERY M. Microstructural evolution during partial remelting of Al-Si7Mg alloys [J]. Materials Science and Engineering A, 1995, 203: 1−13. DOI: 10.1016/0921-5093(95)09861-5.

[37] NIE Shuang, GAO Bing-yang, WANG Xue-jian, CAO Zhi-qiang, GUO En-yu, WANG Tong-min. The influence of holding time on the microstructure evolution of Mg-10Zn-6.8Gd-4Y alloy during semi-solid isothermal heat treatment [J]. Metals, 2019, 9: 420. DOI: 10.3390/ met9040420.

[38] ZHANG Liang, CAO Zhan-yi, LIU Yong-bing. Microstructure evolution of semi-solid Mg-14Al-0.5Mn alloys during isothermal heat treatment [J]. Transactions of Nonferrous Metals Society of China, 2010, 20: 1244−1248. DOI: 10.1016/S1003-6326(09)60286-7.

[39] HEYME H N, SHEVCHENKO N, LEI Z, ECKERT K, KEPLINGER O, GRENZER J, BECKERMANN C, ECKERT S. Coarsening evolution of dendritic sidearms: From synchrotron experiments to quantitative modeling [J]. Acta Materialia, 2018, 146: 176−186. DOI: 1016/j.actamat.2017.12.056.

(Edited by YANG Hua)

中文导读

铸态 AZ31-*x*Gd 镁合金在半固态等温热处理中显微组织和富 Gd 相的演变

摘要：本文深入研究了铸态 AZ31-*x*Gd (*x*=0，1.5 wt%，2.0 wt%，2.5 wt%)镁合金在半固态等温热处理中显微组织和富 Gd 相的演变。结果表明，添加 Gd 的 AZ31 镁合金中的层状 $(Mg,Al)_3Gd$ 相在半固态等温热处理过程中转变为颗粒状 Al_2Gd 相，导致形成更多的球状 α-Mg 晶粒。当 Gd 含量为 2.0%(质量分数)时，半固态球状晶粒的尺寸达到最小值。晶粒细化的主要机理在于树枝晶的重熔以及少量充当孕育剂的 Al_2Gd 相的辅助作用。同时，固液界面处富集的 Al_2Gd 颗粒可以显著阻碍 α-Mg 晶粒的粗化长大。与铸态 AZ31 镁合金(280 MPa)和半固态 AZ31 镁合金(209 MPa)相比，经过等温热处理的半固态 AZ31-2.0Gd 镁合金具有适中的压缩变形抗力(230 MPa)，实现了变形阻力的降低。

关键词：镁；显微组织；稀土元素；Al_2Gd 颗粒；半固态等温热处理